Advanced Ceramics Progress: Vol. 11, No. 2, (Spring 2025) 1-11

Materials and Energy Research Center
MERC

Contents lists available at ACERP

Advanced Ceramics Progress

Journal Homepage: www.acerp.ir

Original Research Article

K, Ca, and Zn Ratios Affect Glass Frit Properties

Aida Faeghinia [a]*, Zahra Khakpour [b], Razieh Salami [c], Mohamad Zakeri [a]

[a] *Associate Professor, Department of Ceramic, Materials and Energy Research Center, Karaj, Iran.*
[b] *Assistant Professor, Department of Ceramic, Materials and Energy Research Center, Karaj, Iran.*
[c] *MSc, Department of Ceramic, Materials and Energy Research Center, Karaj, Iran.*

* Corresponding Author Email: a.faeghinia@merc.ac.ir (Aida Faeghinia)
URL: https://www.acerp.ir/article_225920.html

ARTICLE INFO

Article History:
Received 01 December 2024
Received in revised form 16 April 2025
Accepted 20 July 2025

Keywords:
Glaze,
ZnO,
Size,
Frites,
TEC

ABSTRACT

Frites with mole fractions of 2.5 SiO_2, 0.20 Al_2O_3, 0.15 B_2O_3, 0.15 ZnO, 0.17 K_2O, and 0.67 CaO were studied at three different S ratios—0.37 (denoted as F1 frits), 0.31 (F2), and 0.24 (F3)—where S = K_2O / (CaO + ZnO). ZnO powders of two different particle sizes were used as raw materials: 500 nm (N series), obtained from recycled Zn ingot dust, and >1 µm (F series), sourced from commercial ZnO. Upon decreasing the S ratio, the molar volumes of the frits decreased. The glass transition temperature difference (ΔTg = –154 °C) decreased, whereas the crystallization temperature difference (ΔTp = +17 °C) increased. It was shown that the glass stability (GS) values were independent of ZnO powder size, although the molar volumes of the N series were lower than those of the F series. Crystalline phases identified in the resulting glazes included zinc silicate (willemite), anorthite, and parawollastonite. The hardness values ranged between 700 and 850 Hv, while the glazes exhibited transparency and whiteness values exceeding 80 and 60, respectively.

https://doi.org/10.30501/acp.2025.491648.1172

1. INTRODUCTION

Zinc oxide (ZnO) is an environmentally friendly and technically essential semiconductor (Demir et al., 2006). In the production of transparent ceramic frits, CaO acts as a fluxing agent, contributing to vitrification and transparency, as discussed in CRT applications involving transparent frits (Karaahmet et al .,2019). The ZnO–CaO–Al_2O_3–SiO_2 system is widely used in the industry to produce transparent and glossy glazes (Rudkovskaya et al., 2001).

In the case of ZnO application in glazes, it has been shown (Cabral et al.,2010) that in smaller quantities, ZnO acts as a flux. It functions effectively in glazes with high contents of SiO_2 and Al_2O_3, enhancing gloss and improving the performance of opaque glazes. However, ZnO is expensive, and many attempts have been made to modify glaze formulations to reduce its amount (Melchiades et al., 2010, Partyka et al., 2016 , Oytaç et al. 2016). Recent research (Melchiades et al., 2010) demonstrated that glazes rich in ZnO tend to crystallize in the calcium silicate form; this phase formation can be avoided by adding alumina in amounts ranging from 2 to 4 wt.%. Additionally, the alumina source in this study, supplied from kaolinite, increased the resulting glaze transparency. Another study (Partyka et al., 2016) showed that by blending two transparent and opal frits, the ZnO content was reduced to 0.5 wt.%; however, the density and crystalline phases of these frits were not discussed. Furthermore, a study (Oytaç et al. 2016) demonstrated that substituting zircon for zinc oxide improves the mechanical properties of the glaze, although zinc oxide plays an essential role in controlling whiteness. The tests showed that a whiteness of up to 85.7% and a bending strength of 47.61 MPa were

Please cite this article as: Faeghinia, A., Khakpour, Z., Salami, R., & Zakeri, M. (2025). K, Ca, and Zn Ratios Affect Glass Frit Properties, *Advanced Ceramics Progress*, 11(2), 1-11. https://doi.org/10.30501/acp.2025.491648.1172

obtained at the maximum zircon amount (14.5 wt%) with a low ZnO content (2.5 wt%).

Willemite (Zn_2SiO_4) and gahnite ($ZnAl_2O_4$) are the main crystalline phases in ZnO–CaO–Al_2O_3–SiO_2 glazes, which form with different morphologies. The kinetics of seed formation and growth of willemite and gahnite crystals in such materials have been widely reported (Casasola et al., 2012. Partyka et al., 2025). Another study examined glazes with varying Na_2O/K_2O ratios and found that an increased amount of K_2O lowers the characteristic temperatures of the glazes, suggesting a stronger fluxing effect. This change in fluxing behavior can influence the transparency and surface properties of the glaze (Partyka et al., 2025).

On the other hand, the application of nanoparticles in glazing systems has been developed to achieve unique surface properties in the floor and wall tile industry (Diaz et al., 2014). Incorporating nanoparticle technology has attracted greater attention in ceramic products by yielding outstanding properties (Shaohua et al., 2013). The use of ZnO nanoparticles (NPs), however, has raised serious concerns regarding their fate, transportation, and toxicity in the environment. In the glass industry, zinc oxide is used as a modifier that can dissolve faster than alkaline oxides and reduce the viscosity of glass in the Tg temperature range (Shelby, et al., 1987).

It has been demonstrated that the major effects on melting kinetics and significant variations in reaction paths are directly attributable to the particle size distributions of the components (Bernardin et al., 2009). In this work, a fine grain size sample was prepared by upgrading the halide-bearing zinc oxide concentration from recycling Zn ingot dusts (Melchiades et al., 2009). However, the effect of the mixture of alkaline oxides and zinc oxide has not been investigated. Therefore, this study focuses on ZnO compounds with two different particle sizes (sources) across various K_2O / (CaO + ZnO) ratios to determine how ZnO particle size distribution influences glass melting, frit density, and the final color of the glazes. The characteristics of the frits (crystallization and molar volume) and the resulting glazes were studied. Several transparent frit formulations containing synthetic and commercially available ZnO powders in varying amounts were prepared under laboratory conditions. The physical properties of glazes containing 500-nanometer and 1-micrometer ZnO powders—including density, glass-forming ability, crystalline phases, glass stability, FT-IR, hardness, and color—were compared.

2. MATERIALS AND METHODS

Fine ZnO powder was produced at laboratory scale through a sustainable and environmentally friendly process by upgrading halide-bearing zinc oxide (HZO) concentrate. Initially, the chemical, mineralogical, and physical properties of this nano-ZnO and a commercially sourced standard ZnO were characterized in Figure 2. Subsequently, six frit compositions containing different ZnO powders and various S = K_2O / (CaO + ZnO) ratios were prepared under laboratory conditions. The frit compositions (in wt.%) were selected based on reference (Seo et al., 2009), as these types of glasses are prone to phase separation. The chosen compositions correspond to the center of the compositional triangle proposed by (Seo et al., 2009) to avoid the formation of opalescence (Figure 1).

The frit compositions were 2.5 SiO_2, 0.20 Al_2O_3, 0.15 B_2O_3, (0.15 + x) ZnO, (0.17 + y) K_2O, and (0.67 – z) CaO (in mole fraction) (According to Table 1). The raw materials used for the frits included K_2CO_3 (Merck, Art No. 7734, Germany), $CaCO_3$ (Merck, Art No. 5828, Germany), Al_2O_3 (Merck, Art No. 5550, Germany), B_2O_3 (Merck, Art No. 7783, Germany), ZnO (CAS Number: 13463), and pure optical-grade silica (Azandarian Mining Company, Iran). The batches were mixed in an agate mortar and melted in a platinum crucible at temperatures ranging from 1450 to 1550 °C.

The melts were held for two hours and then quenched in cooled water. The resulting frits were ground using fast milling, screened with 400-mesh sieves, and then mixed with different additives to prepare a slurry with a density of 1.5 g/cm³. Table 2 shows the weight percentages of the additives used to make the slurry. Subsequently, the resulting slurries were sprayed onto fired commercial wall tiles. Firing was carried out at 1070–1160 °C for 3 minutes (Wang et al., 2009), with a total firing time of 90 minutes. The heat treatments were carried out in a tubular furnace. Differential Thermal Analysis (DTA) was performed on 60 mg of frit powder heated at a rate of 10 °C/min up to 1200 °C in a platinum crucible under air atmosphere (model: Netzsch, Germany). Al_2O_3 was used as the reference material. The inflection point of the endothermic drift on the DTA curve was reported as the glass transition temperature (Tg) (Diaz et al., 2014). X-ray diffraction (XRD) analysis was conducted using a PHILIPS PW3710 advanced diffractometer with Cu Kα radiation (λ = 1.5404 Å).

Dilatometer softening point (Td) and coefficient of thermal expansion (CTE) measurements were performed using a dilatometer (model: Netzsch 402E, Germany). Microhardness testing was conducted using the indentation technique with a Vickers indenter (model: MVK-H21). A 100 g load was applied for 15 seconds, and the reported values represent the average of 10 measurements. Prior to testing, sample surfaces were polished with 3 µm alumina powder to obtain a smooth surface. Scanning Electron Microscopy (SEM) observations and Energy Dispersive X-ray (EDX) analyses were performed using a JEOL JXA-840. Samples were mounted on holders, polished, etched, and gold-coated before SEM examination.

TABLE 1. The wt. % of oxides in F1, F2 and F3 systems

Frites composition	K_2O	SiO_2	Al_2O_3	B_2O_3	CaO	ZnO	K_2O/ CaO+ ZnO
F1	7.5	60.1	8.2	4.2	12.7	7.1	0.37
F2	6.5	60.1	8.2	4.2	15.2	5.8	0.30
F3	3.5	60.1	8.2	4.2	17.7	4.3	0.24

TABLE 2. wt. % of additives used in slurries

The additive	Water	Clay	CMC
Weight percent	40	5	0.5

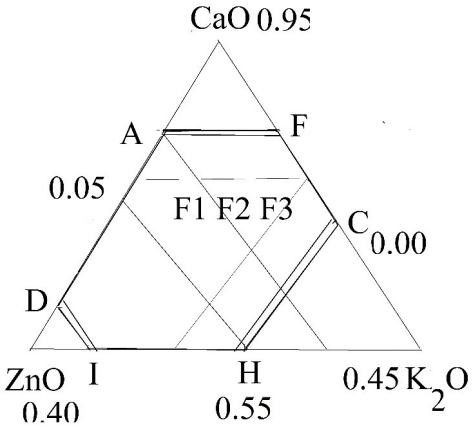

Figure 1. The F1,F2, F3 compositions were selected from the center of compositional triangle proposed by (Melchiades et al.,2014)

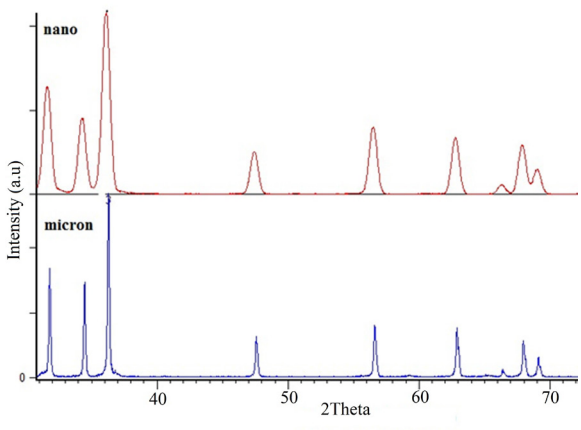

Figure 2. The XRD patterns of the (a) nano–synthesized (b) commercial ZnO

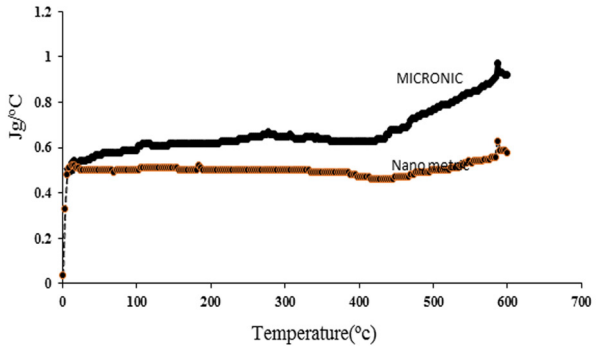

Figure 3. The Cp values of Nano and micro size of used ZnO powder measured by DSC

As expected, in Figure 3 the synthesized powder treated at temperatures above 600 ºC exhibited a specific heat capacity at least 0.4 $J \cdot g^{-1} \cdot ºC^{-1}$ lower than that of the commercial powder. This difference may lead to distinct thermal behaviors in the resulting glaze, which will be discussed later. The morphologies and particle size distributions of both powders were also evaluated. However, due to agglomeration observed in the nanosized powder during Malvern particle size analysis (PSA), the exact particle sizes could not be precisely determined. Nonetheless, the analysis provided a general overview of the particle size distribution. Figure 4 illustrates the PSA results of the powders used.

However, it is evident that the synthesized ZnO powder exhibits a narrow particle size distribution, with over 40 vol.% of the powder particles smaller than 1 micron. The molecular weights of the frites were also calculated as described. Using these molecular weights along with the measured densities, the molar volumes of the frites were determined using the following equation:

$$V_m = \frac{M}{\rho} \quad (1)$$

Here, Vm is molar volume, ρ the density of the sample, and M the molecular weight of the sample. Helium was measured using Pycnometry. FTIR spectroscopy FTIR (IRAffinity-1S) was employed for structural characterization and determining the placement of the functional groups. CIE lab parameters L*,a*, and b* were measured using a spectrophotometer (Hunter lab MiniscanMSXP 4000, 400–700 nm, white glazed tile reference x = 31.5, y 33.3). Here, L* is the lightness axis (black (0) ~ white (100)), b* is the blue (-) ~ yellow (+) axis, and a* is the green (-) ~ red (+) axis.

RESULTS AND DISCUSSION

The XRD patterns of the obtained Frites are presented in Figure 5.The obtained densities, melting temperatures of six series of frites prepared with two different ZnO powder sizes, along with the calculated molar masses and Coefficients of Thermal Expansion (CTE), are summarized in Table 3.

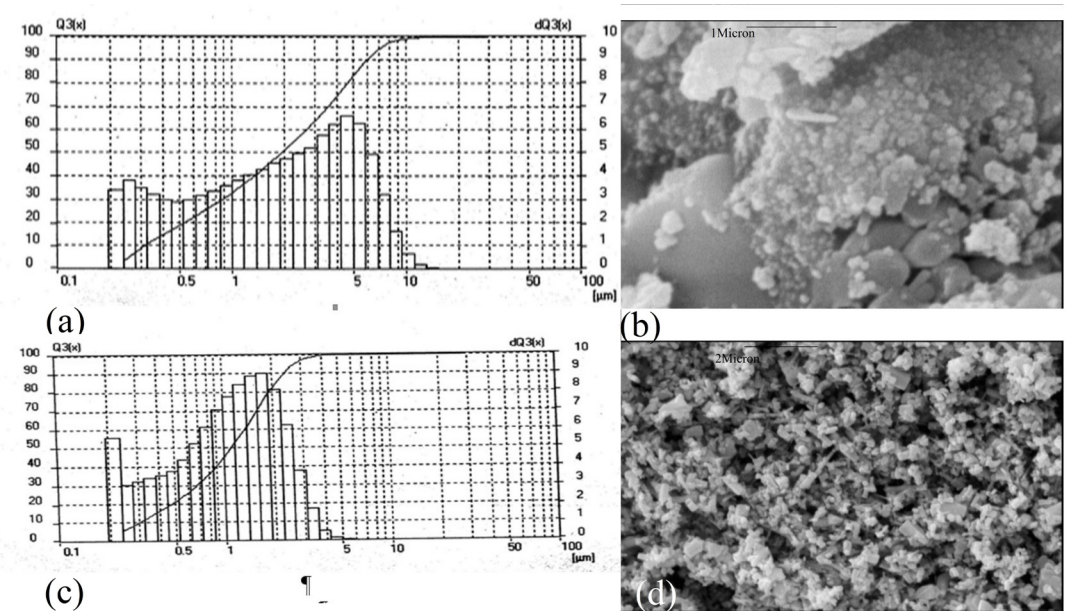

Figure 4. The commercial ZnO powder particle size (b) The SEM micrograph of the commercial ZnO powder (c) The synthesized ZnO powder (d) The SEM micrograph of the synthesized ZnO powder

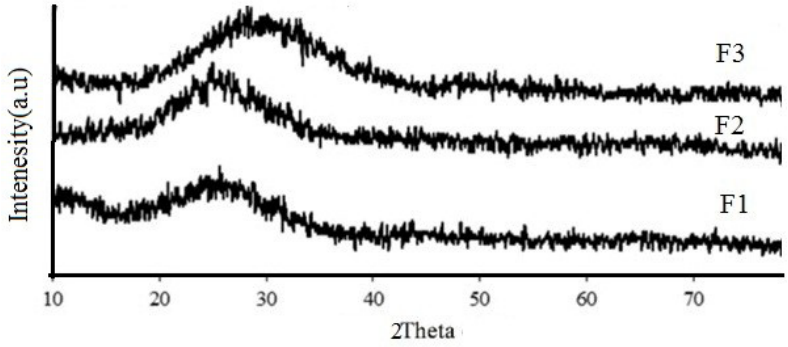

Figure 5. The XRD amorphous pattern of obtained Frite F1, F2 and F3

TABLE 3. The density and melting temperatures of three series of frites

Name	S	Molar mass(g)	Melting tem. ©	Density (g/cm^3)	Molar Volume	CTE×10^{-6}/K
F1	0.37	249.72	1450	2.54±0.0٠1	98.31	6.96±0.01
F2	0.31	246.81	1470	2.55±0.0٠1	96.78	6.88±0.02
F3	0.24	243.52	1550	2.53±	96.25	6.28±0.01
N1	0.37	249.72	1350	2.56±0.0٠1	97.54	-
N2	0.31	246.81	1400	2.58±0.0	95.63	-
N3	0.24	243.52	1450	2.55±0.0	95.4	-

It is evident that increasing the S ratio (from 0.24 to 0.37) leads to a decrease in the melting temperature of the frites (from 1550°C down to 1450°C, respectively). In frites, CaO and K2O typically act as network modifiers (while ZnO can function as either an intermediate or a modifier), and their presence contributes to lowering the melting temperature (Wang et al., 2009).

Figure 6 illustrates the relationship between molar volume and S ratios for the two different particle sizes (PS) of ZnO powder used in the raw material batches.

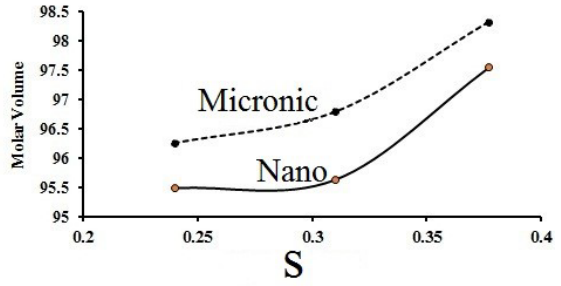

Figure 6. The molar volumes vs. S ratio for two different particle size of ZnO powder.

The Thermal Expansion Coefficient (CTE) values for various S ratios can be predicted using Appen's equation, expressed as follows (Sheckler et al., 1990)

$$f = \Sigma f_i p_i \quad (2)$$

Where pi is the mole fraction of individual oxides and fi is a characteristic expansion factor for each oxide. The values of fi are as follows:
ZnO – 5.0 × 10^{-6}, B2O3 – –5.0× 10^{-6}, SiO2 –3.8 × 10^{-6}, Al2O3 – –3.0× 10^{-6}, CaO – 13.0 × 10^{-6} and K2O – 42.0 × 10^{-6}/K.

It was observed that decreasing the S ratio caused the CTE values of the frites to decrease from 6.28×10-6/K to 6.96×10-6/K. To compare the CTE values of the obtained glazes with that of the tile body, the thermal expansion of the substrate tile was measured, as illustrated in Figure 7a. The difference in thermal expansion between the tile body and the glaze creates mechanical stresses at the interface of these materials

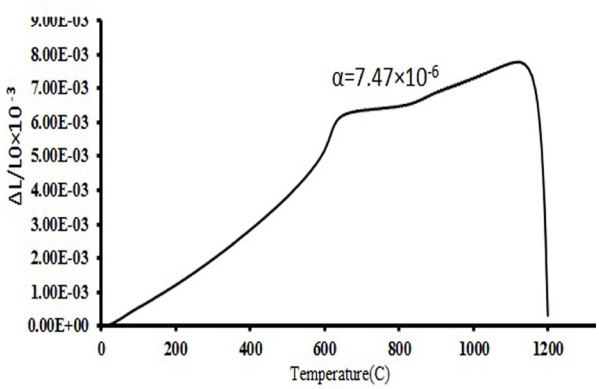

Figure 7a. The dilatometer result of the tile's body

3.2. The DTA Results

The results of the thermal analysis for the obtained frits are compared in Figure 8 and Table 4. The Tg values of the frits were not observed sharply and were recorded over a broad temperature range. Similarly, the crystallization peaks of the samples were not sharp, indicating surface crystallization. However, by differentiating the heat flow curve, the onset of Tg was determined.

TABLE 4. Characteristic temperatures of frites

Characteristic temperatures	T_g °C	T_P °C	T_P-T_g
F1	618	928	310
F2	704	930	226
F3	772	945	173
N1	594	889	295
N2	690	916	226
N3	725	860	135

The compositions (N1-F1, N2-F2, N3-F3) were the same, but the characteristic temperatures differed (the melting temperatures were changed as well). The variation of characteristic temperatures—Tp, Tg, and Tp − Tg—with the S ratio for two different ZnO particle sizes is presented in Figure 7b. A higher glass transition temperature (Tg) in a frit indicates greater stability of its elastic properties (Matori et al., 2010, Kováčik et al., 1999). To compare the glass stability of frits with different ZnO particle sizes and S ratios, the Tp/Tm and (Tp − Tg)/Tm values versus frit compositions are represented in Figure 8c and 8d. Figure 8 shows that the stability of the frits increases as the network modifier content increases.

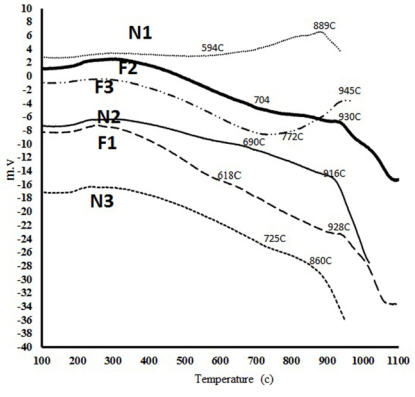

Figure 7b. The DTA results of obtained Frites by 10ºC/min heating rate

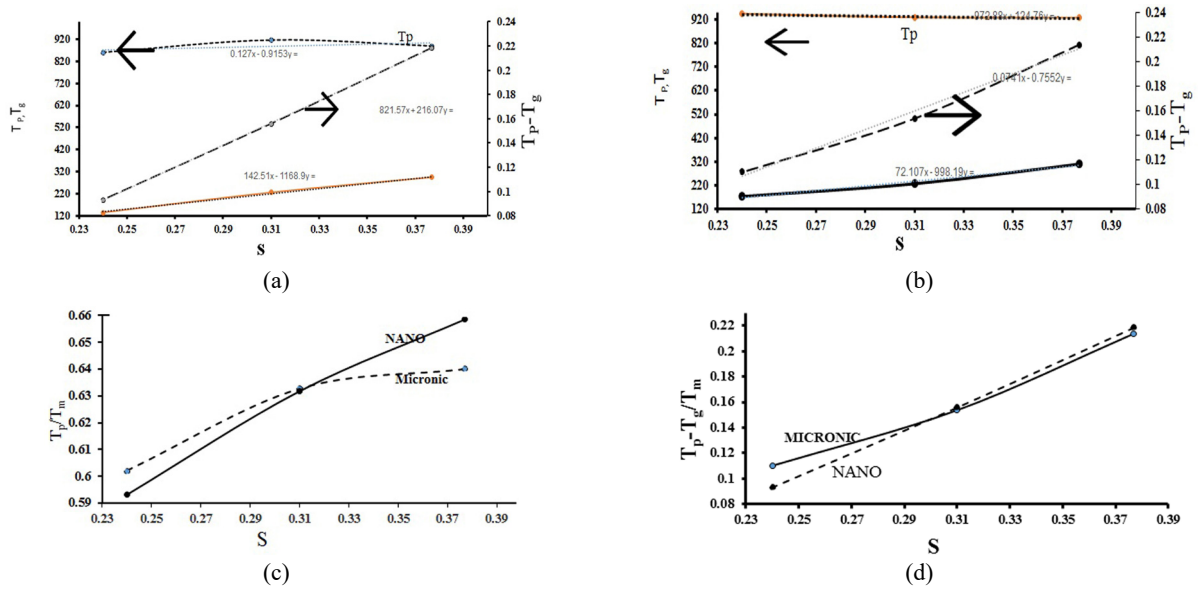

Figure 8. (a)The variation T_p, T_g, T_p-T_g/T_m temperatures by the S ratio in the fine grade system (b) The variation of T_p, T_g, T_p-T_g/T_m temperatures by the S ratio in the Micronics system (c) The T_p/T_m values vs. frites S ratio in micronic and nano ZnO bearing system (d) The T_p-T_g/T_m values vs. S ratio in micronic and nano ZnO bearing system

The results show that frits made with smaller ZnO particles (N series) generally have lower molar volumes compared to those made with larger particles (F series) (Figure 6). This suggests a more compact glass structure when nano-sized ZnO is used. Significance: The more compact structure could potentially lead to improved mechanical properties in the final glaze, such as increased hardness or wear resistance. The glass stability indicators (Tp/Tm and (Tp − Tg)/Tm) show similar trends for both the N and F series across different S ratios (Figure 8c and 8d). This suggests that, while particle size affects melting behavior, it does not significantly impact glass stability.

Significance: This finding is important for glaze manufacturers, as it indicates that nano-sized ZnO can be used to lower melting temperatures without compromising the stability of the glass network.

3.3. FT-IR Evaluation

In Figure 9, the infrared absorption spectra of the experimental frits with different compositions are shown. The absorbance of the spectra was compared to values reported in the literature (Sridhar et al.,T.2020 Chanshetti,et al., 2011 , Ana, et al.,2012). In detail, the IR bands are identified as follows: the Si–O (stretching) mode is located in the range 1000–1200 cm^{-1}, and the Si–O (bending) mode appears around 800 cm^{-1}. The band at 650 cm^{-1} is assigned to the symmetric stretching vibration of Si–O– (Si, Al) between the tetrahedra in the N3 and F2 samples. As the alkali oxide (K_2O) content increased (in the F1 sample), the position of the maximum absorbance of the Si–O (stretching) band shifted towards lower values, down to 1044 cm^{-1}. This suggests that, while ZnO particle size affects melting behavior and some physical properties, it does not fundamentally alter the glass network structure(Zanotto, et al., 1985). This finding supports the idea that nano-sized ZnO can be used as a direct replacement for larger particles in frit formulations without causing major structural changes. In the broader context of ceramic glaze technology, these results highlight the potential of using nano-sized ZnO for optimizing frit and glaze production. Lower melting temperatures could lead to energy savings and potentially allow for lower-temperature firing cycles. The differences in physical properties and crystallization behavior offer new possibilities for tailoring glaze characteristics for specific applications.

3.4. Sintering of resulted glazes

A series of sintering conditions at slow and high cooling and heating rates were done on F and N glazes that were applied on the fired tile. The sintering temperature must be controlled such that the surface of the glazes does not be phase separation, color change or visible warping. Firing temperatures were increased up to 1180 ºC to achieve a gloss appearance on glaze surfaces.

By decreasing the heating rate, diffusivity within the frit increases, which in turn promotes phase separation. Conversely, a fast heating rate (90-minute heating time) results in a higher crystallization temperature compared to slower heating rates (150 minutes). Additionally, fast heating rates (e.g., 60 minutes) can cause warping of glazed samples due to thermal gradients within the models. This damage primarily occurs during the cooling phase, as the bisque tends to shrink after rapid expansion, which may not be well matched with the glaze's shrinkage.

3.5 Phase Evaluation

Figure 10 shows the phase evaluations of heat-treated F1, F2, and F3 frits at 1000 °C for 30 minutes, following a heating time of 90 minutes. The heat treatment conditions used and the appearance of the resulting glaze are shown in Table 5. The low crystallinity (indicated by low peak intensity) of the F1 sample is shown in Figure 10. In contrast, the F3 sample (which has higher Trg values) exhibits relative intensities of the characteristic XRD peaks of the wollastonite phase that are three orders of magnitude higher than those of the F1 sample. The phase evolution of the resulting sintered glazes at 1060 °C (with a 3-minute holding time and 90-minute heating duration) on the tile body is presented in Figure 11. The wollastonite phase remains present in the F1 sample at elevated temperature (ΔT = +60). However, in the F2 and F3 samples, the crystalline phase (wollastonite) transforms into calcium aluminum silicate (anorthite), which may be attributed to the low glass stability (GS) of the system. The presence of calcium aluminum silicate (anorthite) was confirmed by Si–O–Al vibrational bands at 650 cm^{-1} in the FT-IR spectra of the F2 and F3 samples. Calcium silicate and wollastonite phases persisted in the N1, F1, and N3 samples upon increasing the temperature, whereas the anorthite phase was detected in the F3 sample. The intensities of the XRD peaks—and thus the crystallization ability—were higher in the F2 and N2 samples compared to the other samples. Although the F1 and N1 compositions contain higher ZnO content, the willemite (zinc silicate) phase was not detected in the F1, N1, F3, and N3 systems.

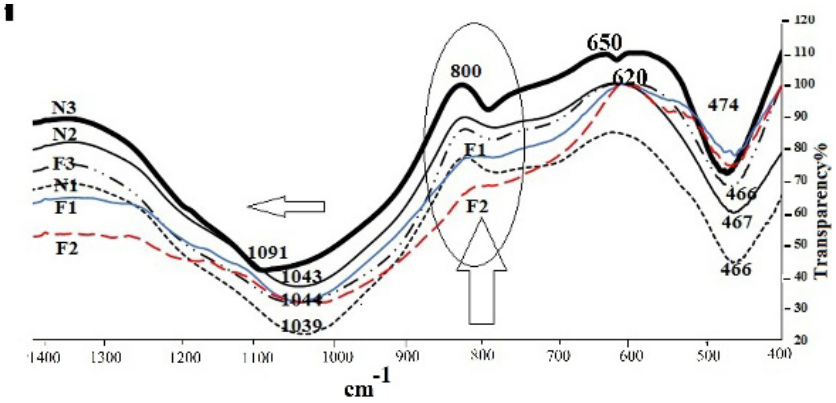

Figure 9. The FT-IR spectrums of F1, F2, F3, N1, N2, N3 frites, the intensity of bending vibration of F2,F1 at 800

TABLE 5. Sintering temperatures and sintering time of obtained glazes with respect to the appearance name

	Sintering temperature°©	60 minute	90 minute	150 minute	210 minute
F1	1060	warping	transparent	opaque	Cracked surface
F2	1080	warping	good	Phase separated(p.s)	Cracked
F3	1160	warping	good	p.s	p.s
F1	1180		Matt-white	Matt-white	
F2	1180	white	Matt-white	Matt-white	Cracked surface
F3	1180	white	white	white	Cracked
N1	1060	Raw glaze	good	-	Cracked surface
N2	1060	Raw glaze	good	-	Cracked
N3	1060	warping	good	-	Cracked surface

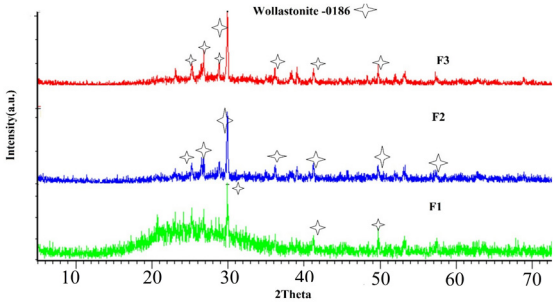

Figure 10. heat treated F1, F2, and F3 at 1000ºC for 30 min. in 90 minutes heating time.

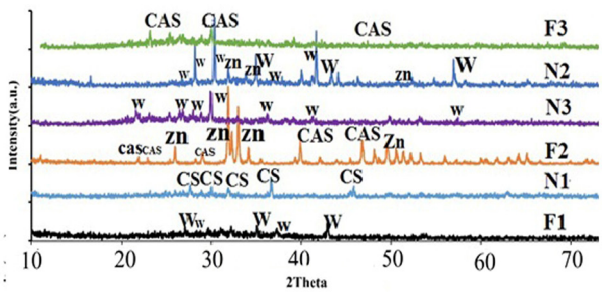

Figure 11. XRD results of heat-treated glazes at 1060ºC for three min. in 90 minutes heating time. (zn; Willemite (zinc silicate), w; wollastonite, CAS; Calcium Aluminum Silicate (Anorthite), CS: (Calcium Silicate)

In contrast, the zinc silicate phase was observed in the F2 glaze, which may be attributed to the formation of ZnO_4 units, as indicated by an FT-IR absorption band at 566.82 cm^{-1}.

3.6 Micro hardness

The resulting Vickers microhardness values and crystalline phases of the glazes are also compared in Table 6.

3.7. Optical Properties

The CIE Lab parameters and gloss values of the F1 to F3 glazes are presented in Figure 12. As shown, the F1 and F2 glazes exhibit high gloss values, while the F3 and N3 glazes show lower gloss unit (GU) values, which correspond to increased calcium silicate crystallization (Sheckler et al.,1990). Additionally, the positive a* value in the F1 sample indicates a slight reddish hue in the glaze. Since the glazes were applied directly onto the tile surface without an engobe layer, the application of a suitable engobe could improve their whiteness. The L* values, along with minimal a* and b* values, indicate a general tendency of both glass-ceramic glazes toward a white appearance. The whiteness index for both was approximately 65%.

3.8. Microstructural Evaluation

The etched and polished surfaces of the samples are shown in Figure 13. All samples exhibit prismatic morphologies, which are characteristic of pyroxene-type minerals such as parawollastonite, anorthite, and calcium silicate. These crystalline phases have thermal expansion coefficients (CTEs) of 7.3×10^{-6}/K, 4.9×10^{-6}/K, and 5.4×10^{-6}/K, respectively. The relatively low CTEs of these crystals contribute to the formation of microcracks around the crystalline phases within the samples.

Needle-like crystals of willemite were also observed in the F2 and N2 samples. By comparing the XRD peak intensities and SEM micrographs of the F1 and N1 samples (Figure 13b), it is evident that their crystalline volume is lower than that of the N3, N2, and F2 samples. Similarly, the F3 sample exhibits noticeably smaller prismatic-like crystals compared to the N3 and N2 samples. High-magnification micrographs are also presented in Figure 13b. Relict morphologies of wollastonite are observed in the F1 and N2 samples. In contrast, the F3 and N3 samples display rounded crystal morphologies, which may be associated with anorthite and parawollastonite, respectively (Shelby et al., 1987).

TABLE 6. The micro hardness and crystalline phases of glazes treated at 1060ºC for 3 minutes with 90 minutes heating time

Name	S	microhardness(Hv)	Crystalline phase
F1	0.377	730±14	Wollastonite
F2	0.31	744±20	Anorthite + Willemite
F3	0.24	817±35	Anorthite
N1	0.377	755±16	Calcium Silicate
N2	0.31	635±-53	Wollastonite+ Willemite
N3	0.24	742±-42	Wollastonite

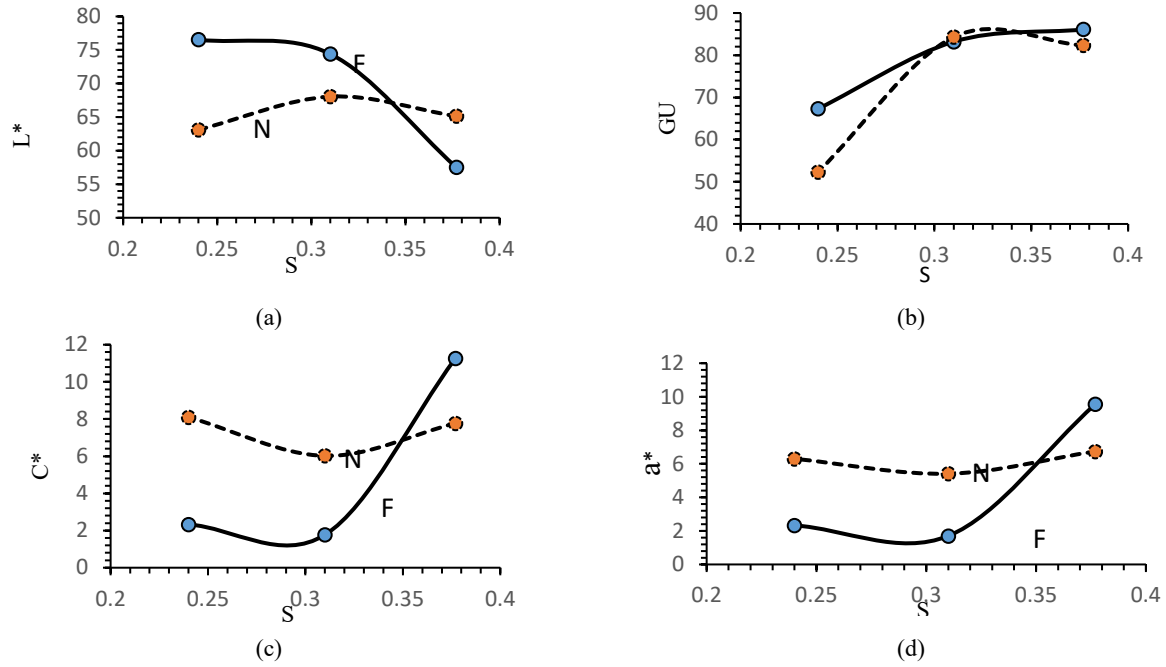

Figure 12. the variation of S values versuse L*(a) GU (b) C* (c) a* (d)

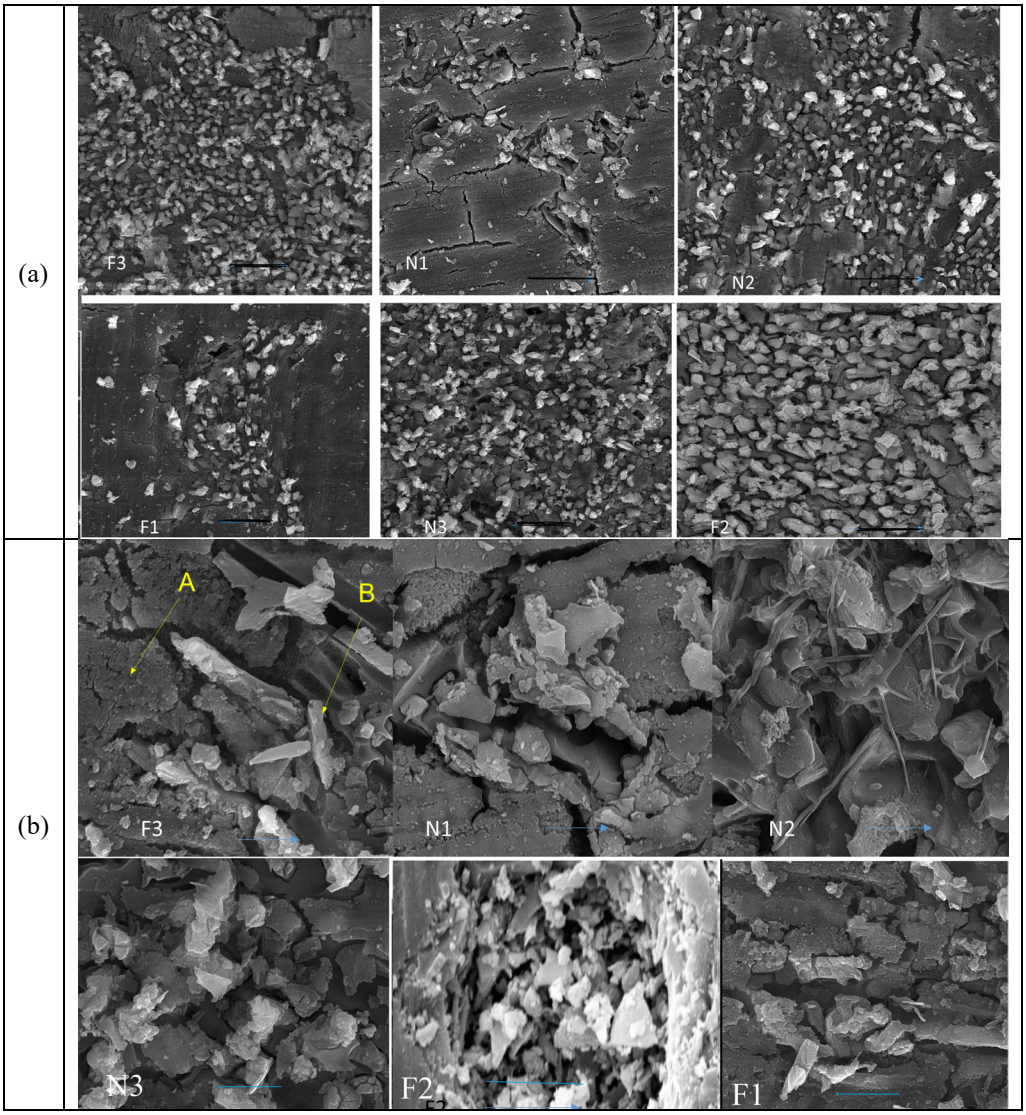

Figure 13. (a) The SEM micrographs of polished and etched glazes by ×2000 magnification(scale bar corresponded to 10μm), (b) The SEM micrographs of polished and etched glazes by ×10000 magnification(scale bar corresponded to 2μm)

4. CONCLUSION(S)

In this work, it was shown that although the ZnO content in the F1 sample was higher than in F3, the role of K_2O as a network modifier was more significant in reducing the melting temperature. This indicates that K_2O can disrupt the glass network more effectively than ZnO and CaO, respectively. K_2O has a lower ionic field strength (IFS) than ZnO and CaO, resulting in a decreased melting temperature (Tm) in F1. Furthermore, potassium ions increase the size of interstices in the glass network, enhancing the free volume. Consequently, the F1 frits exhibit larger molar volumes than the other frits. This increase in volume offsets the atomic weight contribution, leading to a decrease in the overall density of the frit. Additionally, the lower melting and crystallization temperatures in fine ZnO-bearing systems (N-type) may be attributed to the strong physical interactions between ZnO and the silicate chains. Fine ZnO particles possess a lower elastic modulus than pure silicate, which helps arrest the degradation of silicate chains at lower temperatures. This is especially evident with decreasing ZnO particle size in the frit batch.

With an increase in the S ratio (K_2O / (CaO + ZnO)), the glass transition temperature (Tg) increased significantly ($\Delta Tg = 154\ ^\circ C$), while the crystallization temperature (Tp) remained nearly constant or showed a minor increase ($\Delta Tp = 17\ ^\circ C$). The rise in Tg correlates with a decrease in the number of non-bridging oxygen atoms (NBO), resulting in a more rigid glass network.

This finding is consistent with Sheckler & Dinge, who observed that smaller particles accelerate melting in soda-lime-silica glasses. However, this study uniquely correlates particle size with improved energy efficiency (lower Tm) without compromising glass stability (as indicated by Tp/Tm ratios) (Chad, et al., 2005).

Fine-grade frits demonstrate a 30% increase in glass-forming ability (GFA), and stability improves by up to 4.7% in the fine-grade ZnO-bearing sample (N1). It can therefore be stated that fine-grade melts, which have higher viscosities between Tg and Tm, typically exhibit higher GFA and require lower cooling rates. The slope and trend of GFA values ((Tp - Tg) / Tm) in fine ZnO-bearing frits are steeper than those in coarse-grade frits. The increase in stability factor from 0.60 (F3) to 0.64 (F1) is likely due to a decrease in elastic moduli.

However, despite these differences, the firing temperatures between the F and N samples are not significantly different due to only minor variations in their glass stabilities. The F3 sample has higher sintering and crystallization temperatures than the F1 and F2 glazes. Yet, due to its higher K_2O content, the coefficient of thermal expansion (CTE) of the F3 glaze is also higher. The CTE values of the glazes ($6.2–6.9 \times 10^{-6}$/K) are lower than those of the tile body ($7.4–9.9 \times 10^{-6}$/K). When the compressive stress—caused by improper heating time and temperature—exceeds the glaze's strength, warping of the tile-glaze system can occur. This phenomenon was observed in some sintered samples.

The Si–O bending vibration band (around 800 cm^{-1}) decreases in the F1 and F2 frits. A low-frequency band at 466 cm^{-1}, observed in all frit samples (F1, F2, N1, N2), corresponds to the vibration of Zn^{2+} metal cations (Sridhar et al.,(2020). Zinc ions exhibit mixed oxygen coordination numbers of four and five. The interconnections between SiO_4 and ZnO vary: zinc can either act as a network former (in tetrahedral coordination, forming discrete ZnO_4 units) or as a network modifier (in octahedral coordination, disrupting the silica network) (Xiang et al., 2013. , Chad, et al., 2005, Lee et al., 2013). The shift in IR reflection bands related to ZnO in the N3 and F3 samples toward higher wavenumbers suggests tetrahedral coordination of Zn in these systems (Chad, et al., 2005). A weak band at 566.82 cm^{-1} is attributed to the symmetric stretching vibrations of ZnO_4 groups in the F1 and F2 samples. Comparing N1 and N2 samples with F1 and F2, the transmittance bands at 780–800 cm^{-1} shifted to lower values in the N samples, suggesting the formation of ZnO_3 units rather than ZnO_4(Zanotto et al., 1987). In the N1 and N2 samples, the use of nano-sized ZnO may have resulted in premature melt layer formation at low temperatures, which hindered the proper arrangement of Si–O–Zn bonds, as confirmed by FT-IR.

At temperatures above 1000 °C, several processes occur simultaneously, including the disintegration of the wollastonite phase and the crystallization of willemite and calcium aluminum silicate phases in the F2, N2, F1, and N3 samples. The formation of the willemite phase requires the interaction of Zn and Si cations. This interaction is more probable in the liquid phase of the F2 glaze, facilitating diffusion. The F3 glaze exhibits the highest hardness, which is attributed to the presence of the anorthite phase, known for its hardness of 6 on the Mohs scale (Lee et al., 2013). The higher mole fraction of divalent cations in the residual glass phase of F3 and N3 samples also contributes to their increased hardness. In contrast, the F1 and N1 glazes contain a higher percentage of amorphous phase and wollastonite (with a Mohs hardness of 4.4), leading to lower hardness values. Both F3 and N3 glazes exhibit lower gloss values compared to F1. The effective crystallization of anorthite and wollastonite in these glazes reduces surface smoothness, resulting in a white matte appearance. Although the F2 sample contains willemite, the concurrent formation of anorthite likely reduces its gloss.

While (Rudkovskaya et al.,2001)emphasizes willemite (Zn_2SiO_4) as a key phase in ZnO glazes (Lee et al., 2013), this study reports its absence in high-ZnO compositions (F1/N1), attributing this to limitations in ZnO_4 unit formation. This finding contrasts with (Shaohua et al., 2013)who observed ZnO-promoted zircon crystallization (Cheng et al., 2013). The present study also identifies the presence of anorthite ($CaAl_2Si_2O_8$) in the F3 glaze—a phase not previously emphasized in ZnO–CaO–Al_2O_3–SiO_2 systems.

Evaporation of K_2O from the glaze surface results in the transformation of wollastonite into parawollastonite. The lower K_2O content in F3 and N3 samples likely contributes to these phase differences.

In this study, frit compositions consisting of SiO_2, Al_2O_3, B_2O_3, ZnO, K_2O, and CaO were investigated. The S ratios (K_2O / (CaO + ZnO)) in the frit batches were 0.37 (F1), 0.31 (F2), and 0.24 (F3). It was demonstrated that ZnO particle size plays a crucial role in determining the melting point of wall tile glazes. The molar volumes of fine-grade ZnO frits were larger than those of frits with coarser ZnO.

According to DTA results, fine-grade ZnO increases the glass-forming ability compared to samples with micronized ZnO. The glass transition onset is broader in fine-bearing samples, indicating greater thermal stability. Comparing the glass stability of fine- and coarse-bearing ZnO frits, it was found that strength in F1 increased by up to 4.7% compared to N1. Particle size distribution also influences the crystalline phases formed on the tile surface. The fine ZnO-containing glazes (N samples) exhibited wollastonite as the dominant crystalline phase. XRD patterns confirmed that at a K_2O / (ZnO + CaO) ratio of 0.31, both willemite ($ZnSi_2O_6$) and anorthite phases crystallized in commercial ZnO-containing glazes. FT-IR spectra further indicated that the use of nano-sized ZnO may result in inadequate Si–O–Zn bond formation at lower temperatures, a finding supported by XRD analysis.

ACKNOWLEDGEMENT

The author acknowledges the financial support of M.S Project, Contract No. 371398055, received from the Materials and Energy Research Center, Iran.

REFERENCES

1. Ana, K.P., & Šesták, J. (2012). Forty years of the Hrubý glass-forming coefficient via DTA when comparing other criteria in relation to the glass stability and vitrification ability. Journal of Thermal Analysis and Calorimetry, 110(2), 997-1004. https://doi.org/10.1007/s10973-011-1926-6
2. Bernardin, A.M. (2009). The influence of particle size distribution on the surface appearance of glazed tiles. Dyes and Pigments, 80(1), 121-124. https://doi.org/10.1016/j.dyepig.2008.05.011
3. Cabral, A.A., Fokin, V.M., Zanotto, E.D., & Chinaglia, C.R (2003). Nanocrystallization of fresnoite glass. I. Nucleation and growth kinetics. Journal of Non-Crystalline Solids,30(1–3) 15, 174-186. https://doi.org/10.1016/j.jnoncrysol.2003.08.046
4. Casasola, R., Rincón, J.M., & Romero, M. (2012). Glass-ceramic glazes for ceramic tiles – a review. Journal of Materials Science, 47(2), 553-582. https://doi.org/10.1007/s10853-011-5981-y
5. Chad, R. S., &D.M., DeLongchamp (2018). Glassy phases in organic semiconductors. Journal of the American Ceramic Society, 22(2), 41-48. https://doi.org/10.1016/j.cossms.2018.03.001
6. Chanshetti, U.B., Shelke, V.A., Jadhav, S.M., Shankarwar, S.G., Chondhekar, T.K., Shankarwar, A.G., Sudarsan, V., & Jogad, M.S. (2011). Density and molar volume studies of phosphate glasses. Facta Universitatis-Series: Physics, Chemistry and Technology, 9(1), 29-36. https://doi.org/10.2298/FUPCT1101029C
7. Cheng, P., Ming, L., Jianqing, W. (2013). Effect of ZnO on Crystallization of Zircon from Zirconium-Based Glaze. Journal of the American Ceramic Society, 96(7). https://doi.org/10.1111/jace.12441
8. Demir, M., Memesa, M., Castignolles, P., & Wegner, G. (2006). PMMA/zinc oxide nanocomposites prepared by in-situ bulk polymerization. Macromolecular Rapid Communications, 27(10), 763-770. https://doi.org/10.1002/marc.200500870
9. Diaz, P.M., Palanikumar, K., & Kumar, P.R. (2014). Effect of addition of nano zirconia in ceramic glazes. Advanced Materials Research, 984(985), 488-494. https://doi.org/10.4028/www.scientific.net/AMR.984-985.488
10. Karaahmet, O., Cicek, B. (2019). Waste recycling cathide ray tube glass through industrial production of transparent ceramic frits. Journal of the Air & Waste Management Association, 69(10), 1258-1266. https://doi.org/10.1080/10962247.2019.1654037
11. Kováčik, J. (1999). Correlation between Young's modulus and porosity in porous materials. Journal of Materials Science Letters, 18(13), 1007-1010. https://doi.org/10.1023/a:1006669914946
12. Lee, H.S. (2013). The Effect of Nucleating Agent on Zn2SiO4 Crystal Glaze. Journal of the Korean Ceramic Society, 50(2), 116-121. http://dx.doi.org/10.4191/kcers.2013.50.2.116
13. Matori, K.A., Zaid, M.H.M., Sidek, H.A.A., Halimah, M.K., Wahab, Z.A., & Sabri, M.G.M. (2010). Influence of ZnO on the ultrasonic velocity and elastic moduli of soda lime silicate glasses. International Journal of Physical Sciences, 5(14), 2212-2216. Article Number: 8D5B62A33657 https://academicjournals.org/journal/IJPS/edition/4_November_2010
14. Melchiades, G., Rego, B.T., Higa, M.S.M., Helton, J., & Boschi, A.O. (2010). Factors Affecting Glaze Transparency of Ceramic Tiles Manufactured by the Single Fring Technique. Journal of the European Ceramic Society, 30(12), 2443-2449. https://doi.org/10.1016/j.jeurceramsoc.2010.04.030
15. Melchiades, F.G., Neto, C.L., Alves, H.J., & Boschi, A.O. (2009). Formulação de Fritas Cerâmicas com Auxílio da Técnica de Planejamento Estatístico de Experimentos. Cerâmica Industrial, 14(3), 23-29. https://www.ceramicaindustrial.org.br/article/5876573c7f8c9d6e028b4764/pdf/ci-14-3-5876573c7f8c9d6e028b4764
16. Oytaç, Z.E., Atan, E., & Kara, A. (2016). Use of a Sustainable ZnO in Place of Standard ZnO in Ceramic Tile Production. IMMC 2016, 18th International Metallurgy & Materials Congress, 197-203. https://www.academia.edu/77876813
17. Partyka, J., & Leśniak, M. (2016). Preparation of glass-ceramic glazes in the SiO2-Al2O3-CaO-MgO-K2O-Na2O-ZnO system by variable content of ZnO. Ceramics International, 42(7), 8513-8524. https://doi.org/10.1016/j.ceramint.2016.02.077
18. Partyka, J., Kozien, D., Pasiut, K. (2025). The effect of variable ratios of Na2O/K2O oxides in glazes containing BaO, ZnO, ZrO2: Structural analysis and surface properties. Applied Science, 15(2), 648. https://doi.org/10.3390/app15020648
19. Rudkovskaya, N.V., & Mikhailenko, N.Y. (2001). Decorative zinc-containing crystalline glazes for ornamental ceramics (a review). Glass and Ceramics, 58(11-12), 387-390. https://doi.org/10.1023/A:1014958309094
20. Seo, B.H., Kim, H., & Suh, D.H. (2009). Effects of alkali and alkaline-earth oxides on thermal, dielectrical, and optical properties of zinc borate glasses for transparent dielectric. Metals and Materials International, 15(6), 983–987. https://doi.org/10.1007/s12540-009-0983-x
21. Shaohua, W., Peng, C., Lü, M., & Wu, J. (2013). Effect of ZnO on crystallization of zircon from zirconium-based glaze. Journal of the American Ceramic Society, 96(7), 2054-2057. https://doi.org/10.1111/jace.12441
22. Sheckler, A.C., & Dinge, R.D. (1990). Effect of Particle Size Distribution on the Melting of Soda-lime-Silica Glass. Journal of the American Ceramic Society, 73(1), 24-30. https://doi.org/10.1111/j.1151-2916.1990.tb05084.x
23. Shelby, J.E., Bhargava, A., Simmins, J.J., Corah, N.L., McCluskey, P.H., Sheckler, C., & Snyder, R.L. (1987). Atmospheric effects during thermal cycling of Ba2YCu3O7±x superconductors. Materials Letters, 5 (11–12), 420-424. https://doi.org/10.1016/0167-577X(87)90054-1
24. Sridhar, T., Kini, A.U., & Hiremath, A. (2020). Influence of zinc oxide nanoparticles on the mechanical and thermal responses of glass fiber-reinforced epoxy nanocomposites. Polymer Composites, 41(1), 174-181. https://doi.org/10.1002/pc.25357
25. Wang, J.Q., Wang, W.H., Yu, H.B., & Bai, H.Y. (2009). Correlations between elastic moduli and molar volume in metallic glasses. Applied Physics Letters, 94(12), 121904. https://doi.org/10.1063/1.3106110
26. Xiang, Y., Jincheng, D., & Lawrie, D. (2013). Structure and diffusion of ZnO–SrO–CaO–Na2O–SiO2 bioactive glasses: a combined high energy X-ray. RSC Advances, 3(17), 5966-5978. https://doi.org/10.1039/C3RA23231J
27. Zanotto, E.D. (1987). Isothermal and adiabatic nucleation in glass. Journal of Non-Crystalline Solids, 89(3), 361-370. https://doi.org/10.1016/S0022-3093(87)80278-8
28. Zanotto, E.D., & James, P.F. (1985). Experimental tests of the classical nucleation theory for glasses. Journal of Non-Crystalline Solids, 74(2-3), 373-394. https://doi.org/10.1016/0022-3093(85)90080-8